Available online at www.sciencedirect.com

ScienceDirect

Energy Procedia 114 (2017) 693 – 706

Energy Procedia

13th International Conference on Greenhouse Gas Control Technologies, GHGT-13, 14-18 November 2016, Lausanne, Switzerland

Liquid-solid solubility in AMP-KSAR-CO_2-H_2O System

Ugochukwu E. Aronu[a,*], Xiaoguang Ma[b]

[a]*SINTEF Materials and Chemistry, N-7465 Trondheim, Norway*
[b]*Department of Chemical Engineering, Norwegian University of Science and Technology, N-7491 Trondheim, Norway*

Abstract

Solid-liquid solubility of an example novel precipitating solvent system (NPSS); an aqueous blend of AMP and KSAR with and without CO_2 were studied to determine the crystallization and dissolution regimes as well as the nature/composition of precipitate crystals formed. The unloaded aqueous AMP-KSAR solution does not crystallize at 12ºC. Solid crystal formation start at ≈12ºC at loading 0.28mol/mol. Crystals formed for the loaded system was both temperature and loading dependent. Up to medium loading, 0.38mol/mol only one type of precipitate crystal; AMP bicarbonate is formed and the transition dissolution temperature was found to be 46ºC. At high loadings, 0.45 and 0.48mol/mol additional precipitate of potassium bicarbonate ($KHCO_3$) is formed in the mist of the initial AMP bicarbonate precipitate. At loading 0.48 mol/mol the transition dissolution temperature of the $KHCO_3$ precipitate formed is 81ºC.

Peer-review under responsibility of the organizing committee of GHGT-13.

Keywords: Solubility; precipitation; crystallization; dissolution; transition temperature; XRD; SEM; AMP; bicarbonate; amino acid salt

1. Introduction

Capture processes based on liquid-solid phase change during CO_2 absorption have been proposed as a route to reduce cost of capture technology [1]-[2]. Preliminary study of precipitating capture process integrated in an NGCC power plant showed that the capture unit penalty was reduced by 11% compared to MEA [3]. Solubility data for a

* Corresponding author. Tel.: +47 48223272; fax: +47 73596995
E-mail address: ugochukwu.aronu@sintef.no

Peer-review under responsibility of the organizing committee of GHGT-13.
doi:10.1016/j.egypro.2017.03.1212

liquid-solid phase change absorbent system are important parameters for the modeling and design of its CO_2 absorption process. Ma et al., 2012 [4] and Kim et al., 2012 [5] studied the solid-liquid solubility for Pz-CO_2-H_2O system, however not many literatures have studied the behavior of the crystals formed in precipitating absorbent systems. Particularly, to the author knowledge, the crystal nature/morphologies as well as the crystal formation and dissolution regimes of an aqueous blend of amine and neutralized amino acid has not been reported. This work presents solid-liquid solubility study results for a precipitating solvent system from an aqueous blend of an amino acid salt and an amine in-which the amino acid salt activates the formation of an amine bicarbonate precipitate during CO_2 absorption [1]. This precipitating solvent system overcomes some of the challenges of the precipitating processes particularly by increasing the reaction kinetics after precipitation has occurred, thus enhancing its absorption efficiency.

Determination of the crystal formation and dissolution regimes including the metastable zone window for a precipitating absorbent is necessary for the design and operation of such process. The tolerance with respect to sub-cooling during process is related to the metastable zone width (MZW); the temperature difference between the solubility concentration and the supersaturation limit at which spontaneous nucleation occur for a given cooling rate[4]. The corresponding degree of supersaturation will affect both nucleation and crystal growth to give differences in size, shape, and polymorphism of the resulting solid phase, which influence the solid-liquid separation qualities of the resulting slurry in the event of precipitation during CO_2 absorption [4], [6].

Several methods have been applied to detect the onset of crystallization to obtain the metastable zone width including, visualization [7], electrozone sensing [6], ultrasonic measuring technology [8] as well as probes for in situ focused beam reflectance measurement (FBRM) and particle vision measurement (PVM) [9]-[10]. In this work, the metastable zone width and the crystallization and dissolution behaviour as well as the size and shape of the crystal were studied using FBRM and PVM. Solid phase composition was determined by powder X-ray diffraction (XRD) while the crystal morphologies were investigated by scanning electron microscopy (SEM) analysis. The heat for the dissolution of the crystals has been studied [11] to give information on the energy requirements for crystal dissolution.

Nomenclature

T_r	reactor temperature, ^oC
T_j	jacket temperature, ^oC
m'	concentration, mol/kg solution
KSAR	Potassium sarcosine

2. Experimental

2.1 Materials

Chemicals used in this work (Table 1) were used as received without further purification. Aqueous solutions were prepared gravimetrically using distilled de-ionized water. The gases CO_2 (grade 5.0) was supplied by AGA Gas GmbH. An example NPSS, aqueous AMP-KSAR solution was prepared using deionized water by mixing the required amounts of KOH, sarcosine and AMP in a kilogram solution. The amino acid salt (KSAR) is first prepared in the solution by mixing in equimolar proportions of KOH and sarcosine followed by the addition of the required amount of AMP.

Table 1. Chemicals used in this work

Chemical name	CAS number	Purity	Supplier
2-Amino-2-methyl-1-propanol, AMP	124-68-5	99 %	Acros Organics
Sarcosine, SAR	107-97-1	≥ 98.0 %	Fluka
Potassium hydroxide, KOH	1310-58-3	≥ 85 %*	Carl Roth GmbH

* Concentration checked by titration with 1N H_2SO_4

2.2. Crystallization and dissolution regime

The solubility and crystallization studies for the system were carried out in a LabMax® reactor. Detailed description and operating procedure of this apparatus is in [4],[5]. The unloaded aqueous AMP-KSAR solution is charged into the reactor. The solution is then cooled to know the point at which precipitation will occur. Up to 12ºC and at the cooling rate of 1ºC/min no crystal formation was observed both by direct visual inspection and by the online monitoring using the PVM and FBRM instruments. The system was then loaded with CO_2 until crystals were observed upon cooling to ≈12ºC. The system was thereafter subjected to a series of cooling/heating cycles. Crystallization and dissolution of the particles were monitored using optical methods; PVM and FBRM. This process was carried out at five different loadings: 0.28; 0.32; 0.38; 0.45; and 0.48 mol-CO_2/mol-amine. Samples were collected for each loading at designated intervals for loading analysis, XRD and SEM studies of the crystals formed. All data were recorded as function of time.

The transition temperature at which the liquid AMP-KSAR-CO_2-H_2O solution start to crystallize out the first solid upon cooling or the first formed solid crystal is dissolve completely into liquid was determined by at least three cycles of cooling and heating for each loading. The transition temperature for cooling (crystallization) was determined as the temperature at which the heat effect due to phase change was observed on the cooling curve. The heating (dissolution) transition temperature was determined at the temperature where the FBRM count starts continuous decline showing onset of crystal dissolution. Crystals will dissolve completely if the solution is kept at the heat transition temperature.

Cooling/heating rates may have an effect on the transition temperatures [9]. Therefore experiments with different cooling/heating rates, 1, 2, 3; was done at Load 4 (0.28mol/mol) the point at which the first crystals was observed upon cooling to determine possible effects of cooling/heating rate. The experiments were conducted using the jacket temperature (Tj) mode - experimental mode in which the Tj is adjusted to remain constant such that changes in the reactor temperature can readily be monitored to show the heat effect from phase change. A reactor temperature (Tr) experimental mode keeps the Tr constant thus any heat effect due to phase change cannot be observed since the reactor temperature is controlled to be constant.

2.3. Crystal analysis

After each CO_2 loading, the solution in the reactor is cooled to enable solid crystallization from the liquid in a phase change transition. When crystals are formed during cooling, the reactor temperature is set to stabilize at the observed crystallization temperature and a sample of liquid and solid formed is collected as a slurry, the slurry is filtered (to remove the liquid) and dried by vacuum filtration for powder XRD and SEM characterization. Typically, one sample is collected for each loading but in Load 7 additional precipitation was observed thus multiple samples were collected in accordance with the observed crystallization and dissolution temperatures to enable studies on the type of crystals formed at different temperatures. Multiple samples were not collected in Load 8 where a similar phenomenon was observed. Table 2 gives a summary of the sampling temperature for the various samples collected for crystal analysis.

Table 2. Summary of samples collected for Crystal Analysis

Sample	Loading *(mol-CO_2/mol-N)*	Sampling Temperature (ºC)
Load 4	0.28	12.6
Load 5	0.32	24.8
Load 6	0.38	43
Load 7	0.45	44.5, 49, 60, 68
Load 8	0.48	50

3. Results

3.1. Crystallization and dissolution regime

Sample results of online data log for crystallization and dissolution experiments are shown in Fig. 1 and Fig. 2. In Fig. 1 the reactor is cooled (from about 55ºC) in a smooth cooling curve until a phase change reaction takes place, when the accompanying heat effects (heat of precipitation) causes a sharp change in slope resulting in crystallization (precipitate 1). The one-set of precipitation is shown by the sudden increase in the FBRM counts of particles below 1 µm size. The solution remains at the set cool temperature, Tj, (20ºC in this case) for 1hr for complete nucleation and then heated at the set heating rate for dissolution and remains at the set heat temperature, Tj, for about 1hr for complete crystal dissolution. The on-set of crystal dissolution is shown by a sudden decrease in the FBRM count.

Fig. 1 shows that the solution does not maintain a constant temperature at the region of crystallization and also at the dissolution region, this could be due to different thermal properties of the five different compounds in the AMP-KSAR-CO_2-H_2O system mixture. The point of crystallization or dissolution of crystals was therefore monitored using the two online instruments; PVM and the FBRM. *Crystallization* (cooling transition) *temperature* was determined as the temperature at which the heat effect due to phase change is observed on the cooling curve. This is typically observed at the point where the FBRM count meets the cooling curve (Tr). The *dissolution* (heating transition) *temperature* is determined as the reactor temperature, (Tr) at which FBRM count starts to decline. Depending on the loading, it was also possible to observe the formation of different type of crystals within the precipitate as captured in Fig. 2. Upon cooling the loaded sample, a new additional crystallization (precipitate 2) is observed and as the cooling continued another precipitate similar to initial (precipitate 1) is observed as recorded by FBRM. Dissolution of precipitate 1 and precipitate 2 is also seen from the FBRM count log.

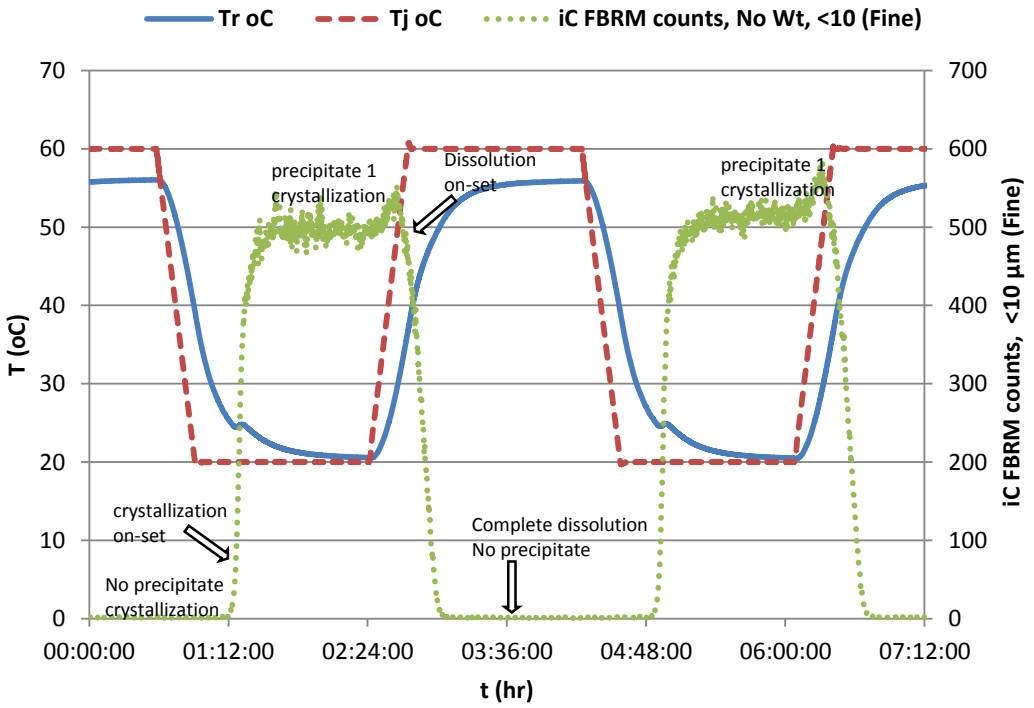

Fig. 1. An example of online temperature curves during cooling and heating of AMP-KSAR-CO_2-H_2O system showing the precipitate and non-precipitate regions at loading 0.28mol/mol

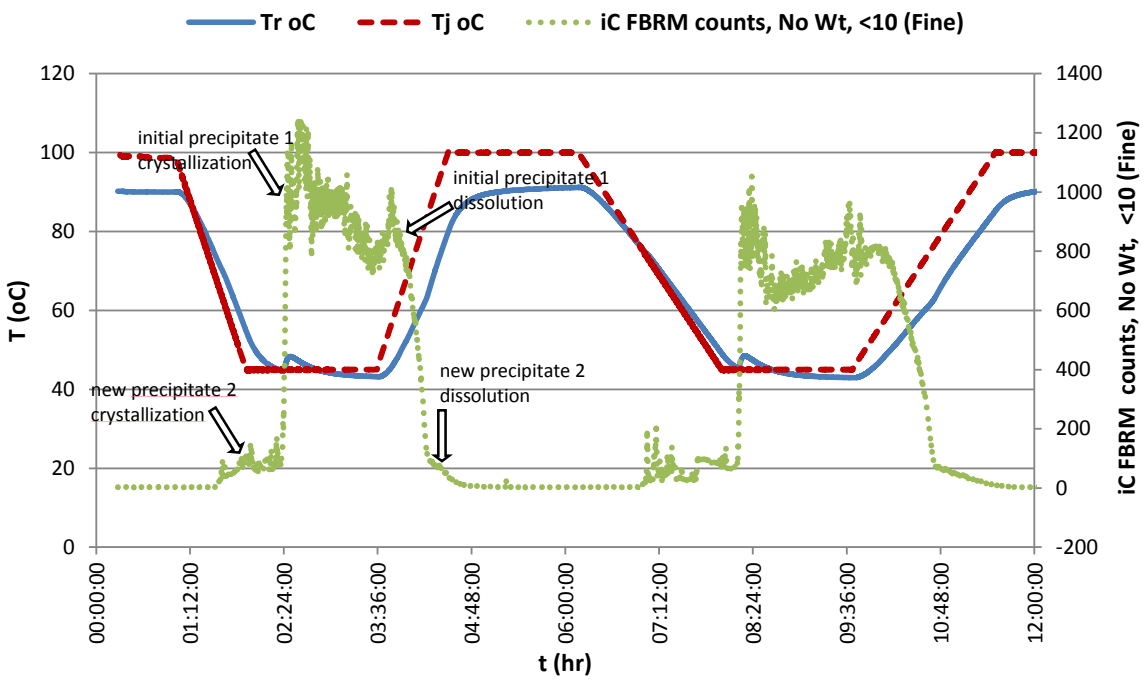

Fig. 2. An example of online temperature curves during cooling and heating of AMP-KSAR-CO_2-H_2O system at the region where 2nd precipitation occurs in the mist of the initial first precipitation.

The result of cool/heating rate test are shown in Table 3 It may be seen from the Table that the different cool/heat rate resulted to same crystallization and dissolution temperatures. It is also observed that the metastable zone width is not adversely influenced by the heating/cooling rate. The rate of 2ºC/min was selected for further experiments in order to reduce the measurement time; similar rate was found adequate by Kim et al., 2012 [5]. A summary of transition temperatures and metastable zone width measured for the AMP-KSAR-CO_2-H_2O system at various loading studied is presented in Table 4.

Table 3 Determination of the effect of cooling/heating rate on the determined transition temperature for AMP-KSAR -CO_2-H_2O system at load 4 (loading 0.28 mol/mol).

Load	Loading (*mol/mol*)	Tj low (ºC)	Tj high (ºC)	Heat/Cool rate (ºC/*min*)	Transition t. (ºC)		Metastable zone width (ºC)
					Cooling	Heating	
4	0.28	10	55	2	13	24.2	11.2
				1	13.3	24.4	11.1
				3	13.4	24.3	10.9

Table 4 Summary of transition temperatures at various CO_2 loading for AMP-KSAR -CO_2-H_2O system.

Load	Loading (*mol/mol*)	Tj low (*°C*)	Tj high (*°C*)	Precipitate 1			Precipitate 2		
				Transition T. (*°C*)		Metastable zone width (*°C*)	Transition T. (*°C*)		Metastable zone width (*°C*)
				Cooling	Heating		Cooling	Heating	
0	0.00	No precipitation							
1	0.06	No precipitation							
3	0.22	No precipitation							
4	0.28	10	55	12.3	24.8	12.5			
				13.0	24.2	11.2			
				12.4	24.6	12.1			
				12.7	24.3	11.6			
5	0.32	20	60	24.6	33.2	8.5			
				24.7	33.6	8.9			
				25.7	34.3	8.6			
6	0.38	35	70	43.9	46.4	2.5			
				42.4	46.3	4.0			
				41.2	44.8	3.5			
7	0.45	45	95	47.7	52.1	4.5	69.0	73.1	4.1
				47.8	53.9	6.1	67.7	74.2	6.5
		45	100	48.3	51.6	3.2	67.7	71.2	3.5
				47.2	50.0	2.9	66.3	71.8	5.5
8	0.48	50	105	49.5	54.2	4.7	79.3	81.0	1.7
				51.3	56.8	5.5	78.2	81.4	3.2
		45	105	48.9	54.1	5.2	76.9	82.0	5.0

FBRM measures the light reflected by particles that pass close to the probe window, and reports these chord lengths as a non-normalized distribution. Chord size distribution gives an estimate of *particle size distribution*. An example of particle size distribution before and after crystallization for the first crystallisation observed (Load 4) is presented in Fig. 3

PVM – in-situ particle vision microscope allows to take images during the experiment. Crystal images taken for the AMP-KSAR system at different intervals during the crystallization studies at different loadings are shown in Fig. 4 – Fig. 7. Fig. 4a shows the first crystallization at Load 4 at 12.3°C with the formation of long needle crystals, the crystal density is seen to increase on cooling to 12.2°C and waiting in Fig. 4b. PVM images for Load 5 are shown in Fig. 5. The figure shows that same needle crystals as in Load 4 were formed, however the crystals are formed at higher temperature, ≈25°C as the loading is increased. The needle crystals found in Load 4 and 5 were identified to be AMP bicarbonate by XRD and SEM analysis (see section 3.2). PVM images was mistakenly not captured in Load 6.

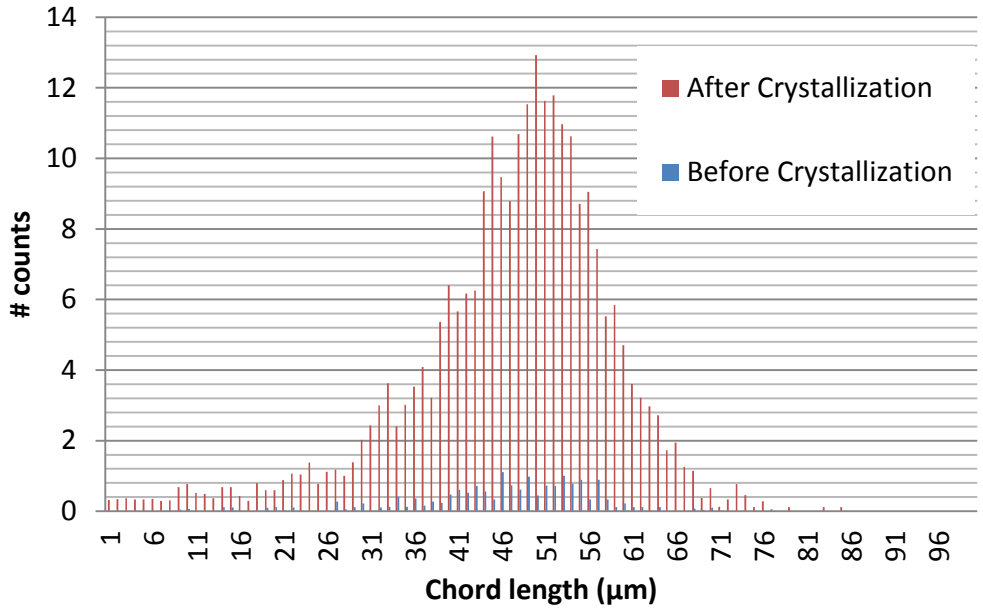

Fig. 3 Example Chord size distribution before and after crystallization.

At Load 7, loading 0.45 mol-CO_2/mol-N; at ≈45ºC a dense mix of precipitate was formed as shown in Fig. 6a, as the slurry is heated up to ≈56ºC a visible mix of long needle and flat rhomboid crystal is observed in Fig. 6b indicating that a new type of precipitate is being formed among the needle crystals. As the solution is heated further to ≈67ºC, the needle crystals are observed to disappear (see Fig. 6c). The rhomboid crystals are observed to disappear at ≈71ºC in Fig. 6d. As the loading is increased further to Load 8, , the PVM images in Fig. 7 show similar behaviour of the crystals as observed in Load 7, the difference is that the transition temperatures occur at slightly higher temperatures than in Load 7. The new type of crystals found in Load 7 and Load 8 among the needle crystals (AMP bicarbonate) have been identified in section 3.2 to be potassium bicarbonate ($KHCO_3$).

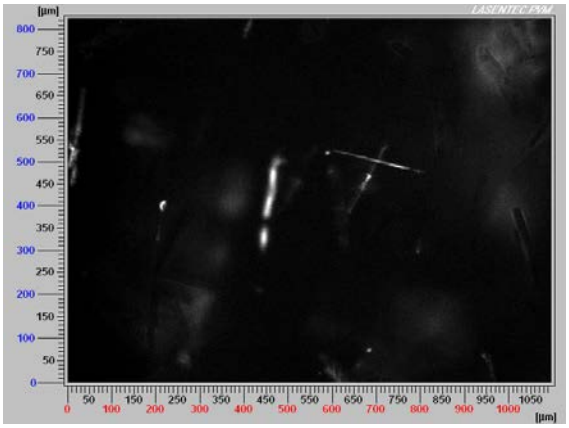

a. Load 4: 12.3ºC on set of crystal formation. Needle crystals formed.

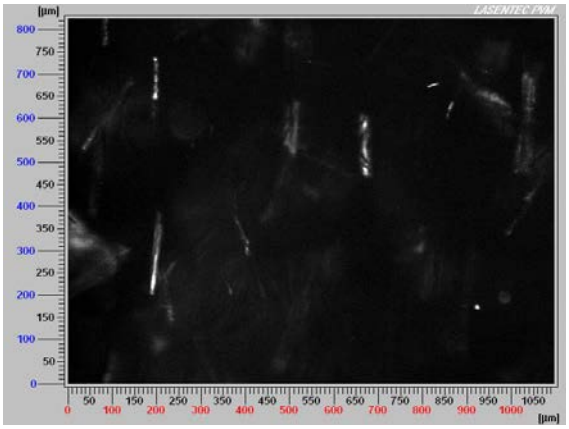

b. Load 4: 12.2ºC increased needle crystal density.

Fig. 4 PVM images at Load 4 (0.28 mol/mol) at ≈12oC showing formation of needle crystals.

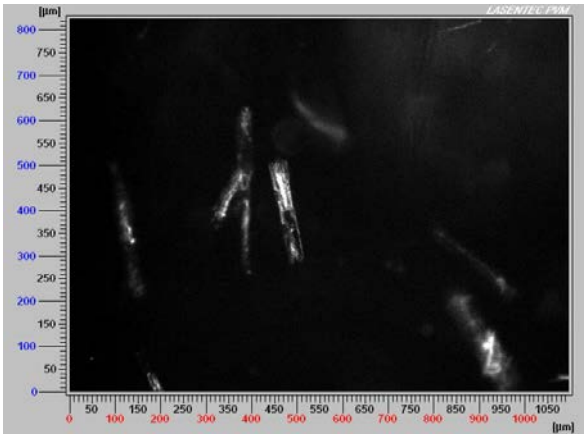

a. Load 5: 24.7ºC on set of crystal formation. Needle crystals formed

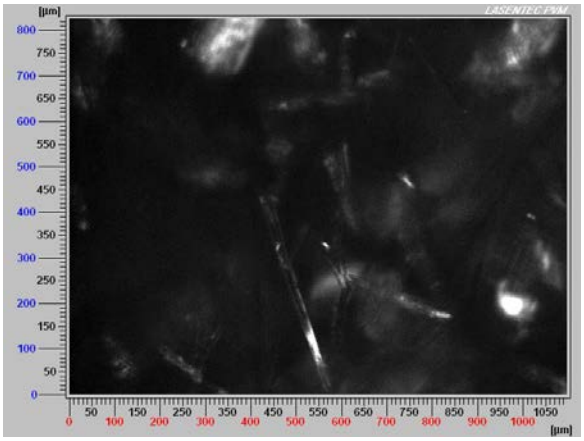

b. Load 5: 24.5ºC increased needle-like crystal density.

Fig. 5 PVM images at Load 5 (0.32 mol/mol) at ≈25ºC showing formation of needle crystals.

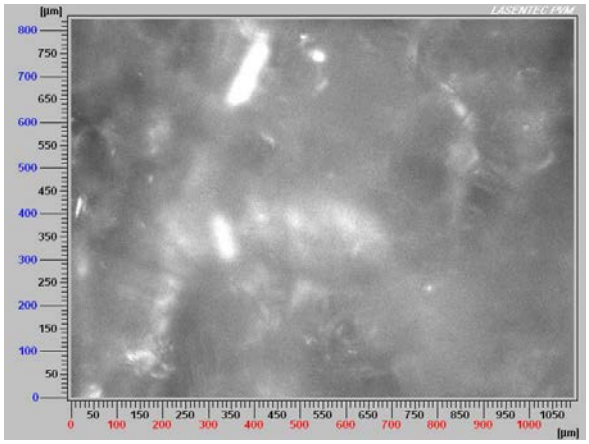

a. Load 7: 44.5ºC Dense mix of precipitate

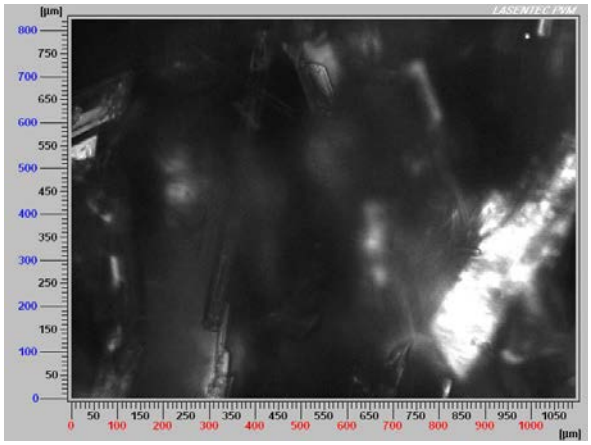

b. Load 7: 55.6ºC. Mix of needle and rhomboid crystals.

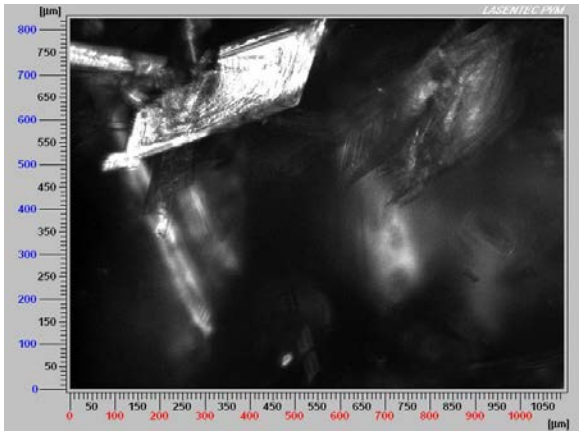

c. Load 7: 67.4ºC. Only rhomboid crystals left

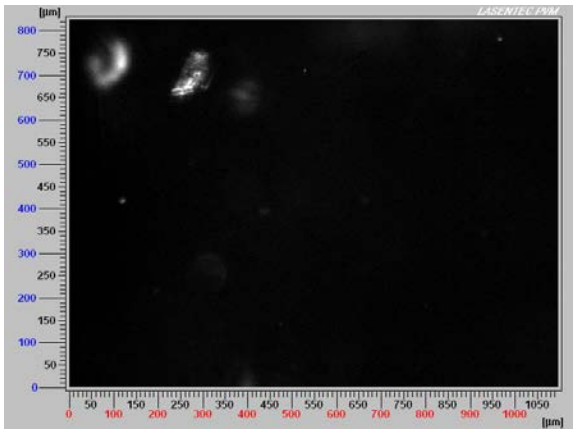

d. Load 7: 71ºC, crystals disappears

Fig. 6. PVM images at Load 7 (0.45 mol/mol) showing formation of mix of needle and rhomboid crystals, with needle crystals disappeared at higher temperature of ≈67ºC.

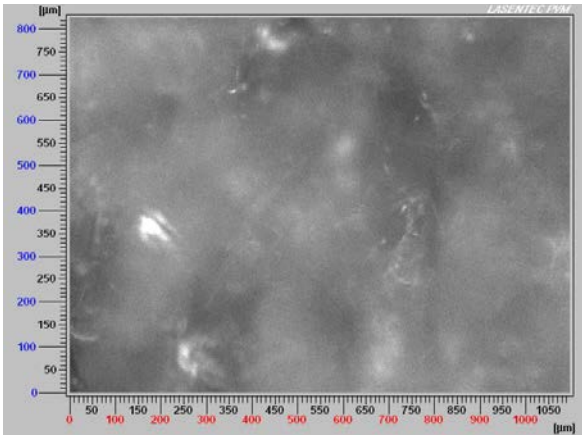

a. Load 8: 51ºC Dense mix of precipitate

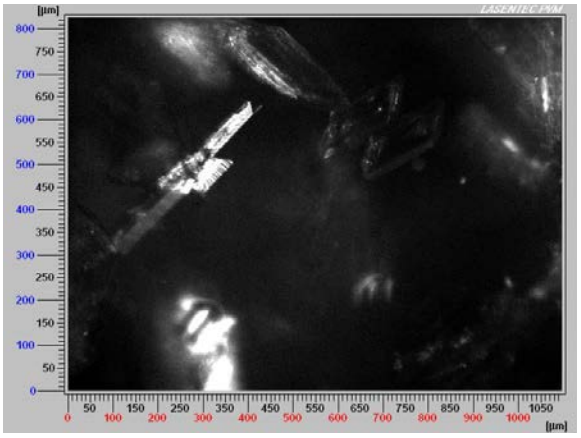

b. Load 8: 57.2ºC. Mix of needle and rhomboid crystals.

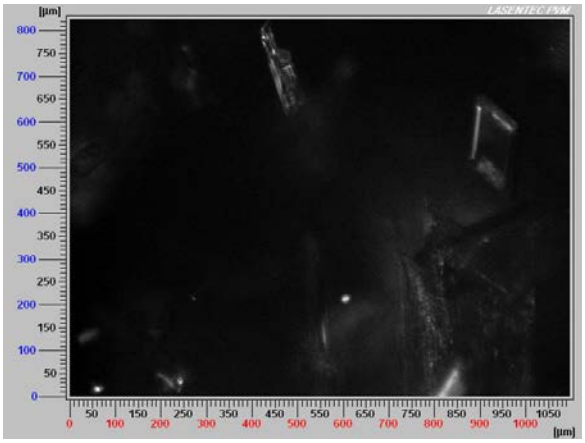

c. Load 8: 68.8ºC. Only rhomboid crystals left

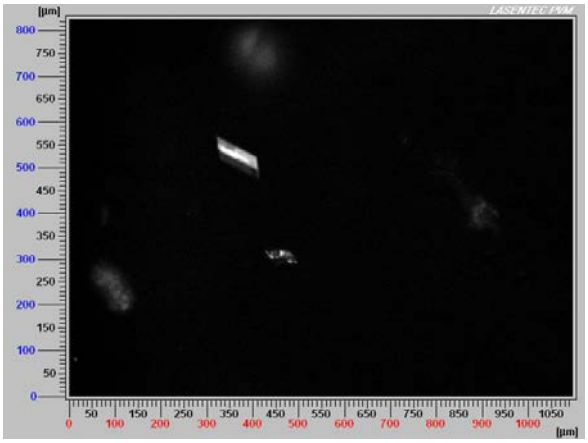

d. Load 8 75.62ºC, crystals virtually disappears

Fig. 7 PVM images at Load 8 (0.48 mol/mol) showing formation of mix of needle and rhomboid crystals, with needle crystals disappeared at higher temperature of ≈67ºC.

The relationship between the transition temperatures and CO_2 loading in AMP-KSAR-CO_2-H_2O system is shown in Fig. 8. The metastable zone is shown as the region between the crystallization and dissolution curves. The figure shows that during the tests the first crystals were formed at loading 0.28 mol/mol at 12ºC and dissolves at 24ºC. The crystallization temperature is then seen to increase with loading and begin to flatten out at loading 0.38 to 0.48mol/mol. At loading 0.45 mol-CO_2/mol-N, new additional precipitation occurs. The new crystals have higher crystallization and dissolution temperatures. The crystallization temperature for the second crystals at this loading is 67ºC and dissolution occurs at 72ºC.

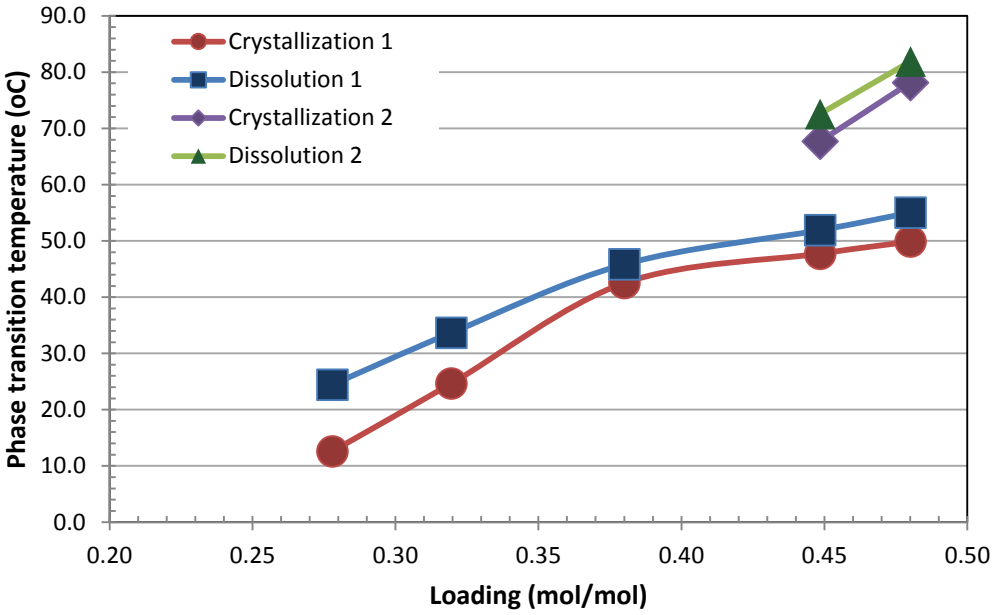

Fig. 8 . Phase transition temperatures curve for crystallization and dissolution for CO_2 loaded aqueous AMP-KSAR solution.

3.2. Crystal analysis

XRD result for reference AMP bicarbonate and crystals from Load 4, 5 and 6 of AMP-KSAR -CO_2-H_2O are shown in Fig. 9. Based on the XRD patterns in the figure, at Loading 4, 5 and 6, it can be observed that only AMP bicarbonate is precipitated when the solution temperature was cooled down to 12.6, 24.8 and 43ºC respectively. The morphologies of the crystals as captured using SEM are shown in Fig. 10 The figure shows that the crystals are of elongated polyhedral shape with the length of over 100 µm, which is beneficial to solid-liquid separation due to the large crystal size.

At higher loading, Load 7, it can be observed from the XRD result in Fig. 11 that a mixture of AMP bicarbonate and $KHCO_3$ was present in the crystals collected. Based on the observation from FBRM count during the experiment, it was decided to sample at different temperatures in Load 7 to enable analysis of the effect of temperature on the different compounds formed. From the XRD results, it is observed that at lower temperature, 44.5 and 49ºC, a mix of AMP bicarbonate and $KHCO_3$ are present in the crystal. However, as the system temperature is increased to 60ºC and further to 68ºC, only $KHCO_3$ crystal is present. AMP bicarbonate is seen to have dissolved at these temperatures (60 and 68ºC) while $KHCO_3$ remain undissolved. The morphologies of crystals precipitated from Load 7 as captured using SEM are shown in Fig. 12 It is difficult to distinguish AMP bicarbonate and $KHCO_3$ using their morphology, but both types of crystals are in large size with the length over 100µm. The precipitated crystals of $KHCO_3$ found at 60 and 68ºC are in the shape of polyhedron. The behavior of the system at Load 8 is very similar to the observed behavior at Load 7. In order words similar precipitate were produced in Load 8 as in Load 7 except that the transition temperatures are slightly higher in Load 8. In summary the crystal analysis show that, only AMP bicarbonate is precipitated at Load 6 and lower loading at the sampling temperatures. At Load 7 and above, two types of precipitate can be found, the first precipitate as the solution is cooled down to 68ºC was $KHCO_3$ and this remained up to about 60ºC. With the further decrease of the temperature down to around 49 °C, AMP bicarbonate started to precipitate, resulting to a more dense mixture of AMP bicarbonate and $KHCO_3$ in the final product at around 44ºC.

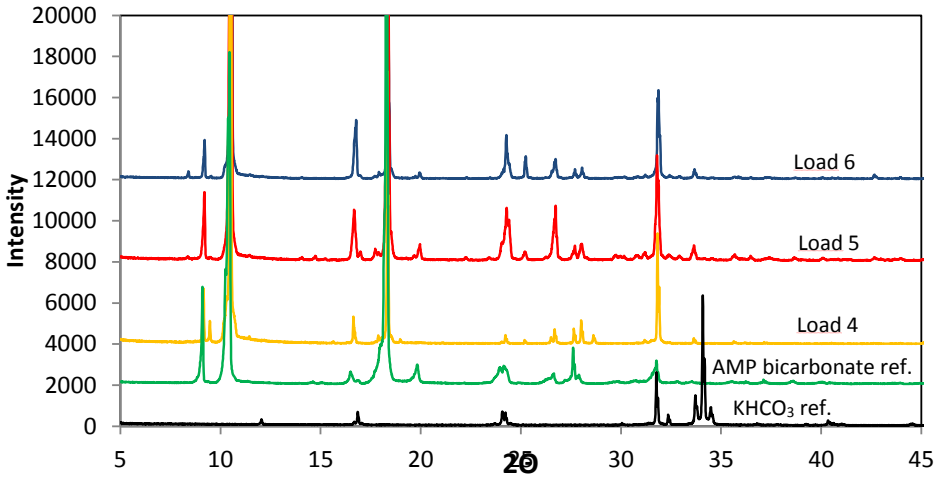

Fig. 9 XRD patterns of the AMP bicarbonate reference crystal (green), crystals obtained after Load 4 (yellow), Load 5 (red) and load 6 (blue).

(a) Load 4: crystal sampled at 12.6°C

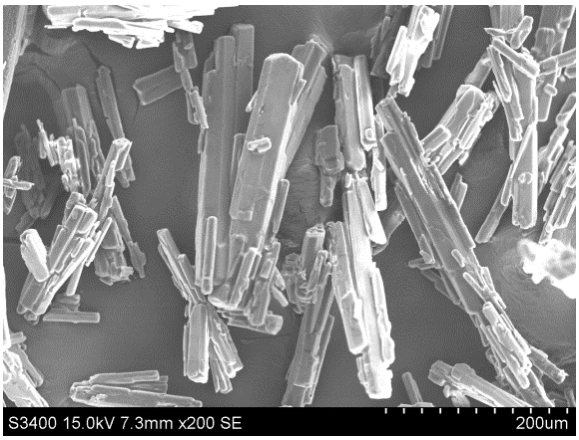

(b) Load 5: crystal sampled at 24.8°C

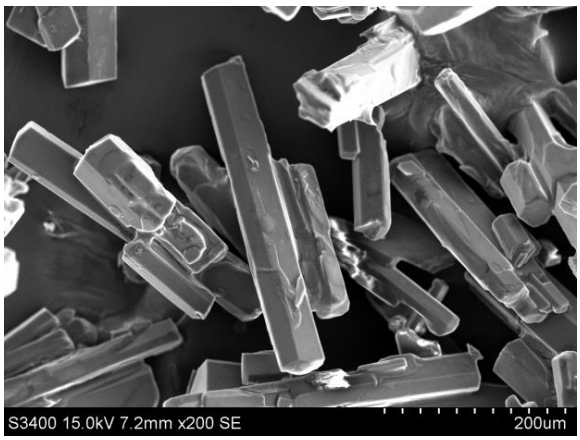

(c) Load 6: crystal sampled at 43°C

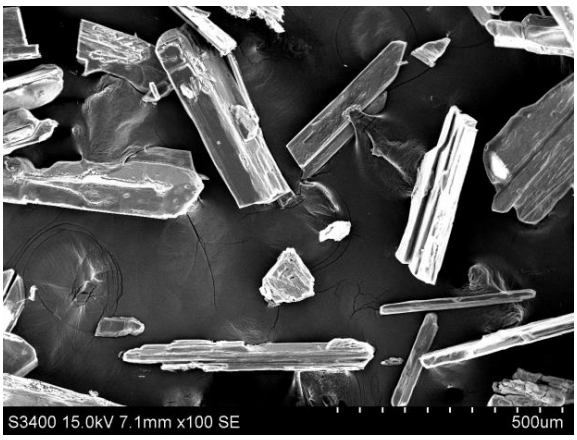

(d) AMP bicarbonate reference

Fig. 10 Morphologies of AMP bicarbonate precipitated from the solutions at (a) Load 4 (b) Load 5 (c) Load 6 (d) AMP bicarbonate reference

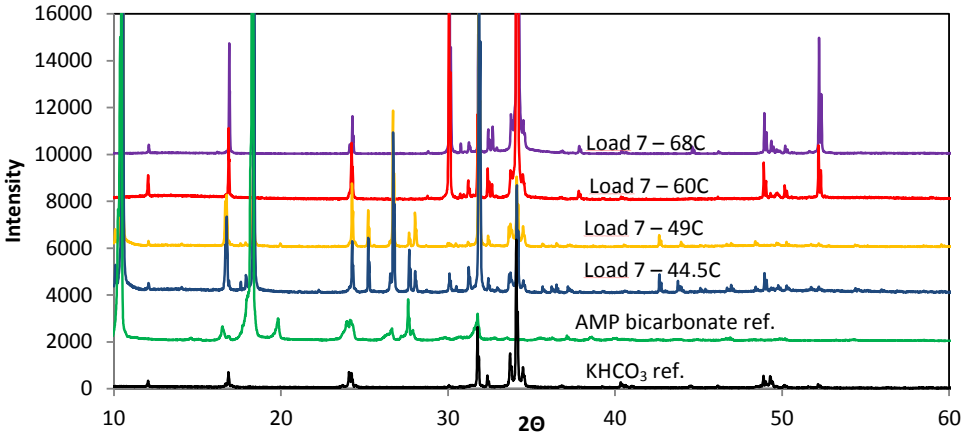

Fig. 11 XRD patterns of crystals precipitated at Load 7- 44.5°C (blue), Load 7- 49°C (yellow), Load 7- 60°C (red), Load 7- 68°C (purple) as well as the reference patterns of AMP bicarbonate (green) and $KHCO_3$ (black)

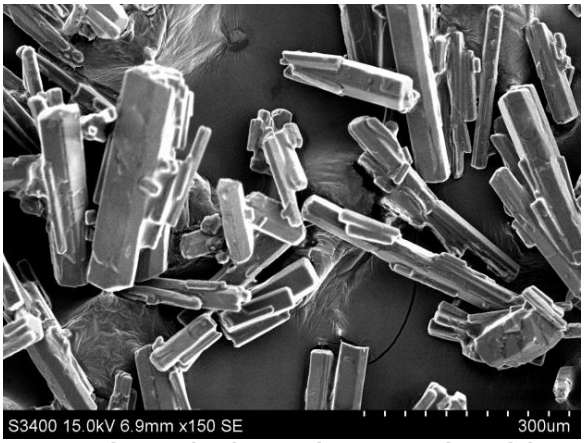

(a) Load 7: AMP bicarbonate and $KHCO_3$ crystals sampled at 44.5°C

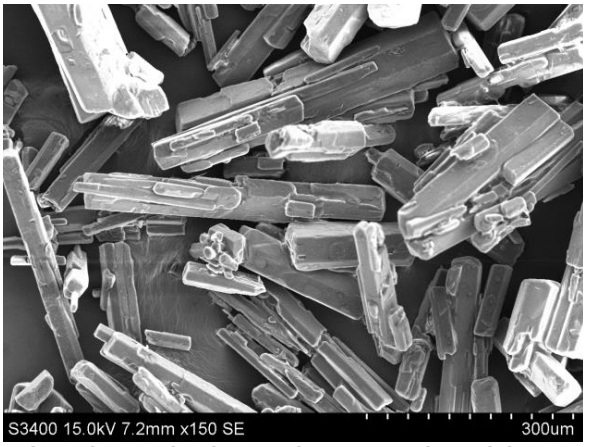

(b) Load 7: AMP bicarbonate and $KHCO_3$ crystals sampled at 49°C

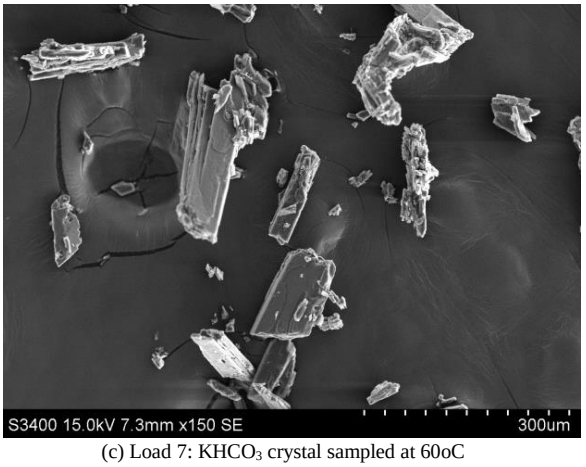

(c) Load 7: $KHCO_3$ crystal sampled at 60oC

(d) Load 7: $KHCO_3$ crystal sampled at 68°C

Fig. 12 Morphologies of precipitated crystals from the solutions of Load 7 at various sampling temperature.

4. Conclusions

Solid-liquid solubility of an example novel precipitating solvent system (NPSS); an aqueous blend of AMP and KSAR with and without CO_2 were studied to determine the crystallization and dissolution regimes as well as the nature/composition of precipitate crystals formed. The unloaded aqueous AMP-KSAR solution does not crystallize at 12°C. Solid crystal formation start at ≈12°C at loading 0.28mol/mol. Crystals formed for the loaded system was both temperature and loading dependent. Up to medium loading, 0.38mol/mol only one type of precipitate crystal; AMP bicarbonate is formed and the transition dissolution temperature was found to be 46°C. At high loadings, 0.45 and 0.48mol/mol additional precipitate of potassium bicarbonate ($KHCO_3$) is formed in the mist of the initial AMP bicarbonate precipitate. At loading 0.48 mol/mol the transition dissolution temperature of the $KHCO_3$ precipitate formed is 81°C

Acknowledgements

This publication has been produced with support from the BIGCCS Centre, performed under the Norwegian research program *Centres for Environment-friendly Energy Research (FME)*. The authors acknowledge the following partners for their contributions: Gassco, Shell, Statoil, TOTAL, GDF SUEZ and the Research Council of Norway (193816/S60).

References

[1] Aronu U. E., Kim, I., Haugen, G. Evaluation of energetic benefit for solid-liquid phase change CO2 absorbents. Energy procedia, Vol. 63, 2014 Pg. 532-541

[2] Sanchez-Fernandez, E., Mercader, F.d.M., Misiak, K., van der Ham, L., Linders, M., Goetheer, E. New Process Concepts for CO2 Capture based on Precipitating Amino Acids. Energy Procedia 2013, 37, 1160-1171.

[3] Aronu , U. E., Kim, I., Haugen, G., Clos, D.P., Jordal, K. Integration of a precipitating CO2 capture process in an NGCC power plant. 3rd Post Combustion Capture Conference (PCCC3) and SaksPower Symposium, Regina, Canada. 8-11th September, 2015.

[4] Ma, X., Kim, I., Beck, R., Knuutila, H., Andreassen, J.-P., 2012. Precipitation of Piperazine in Aqueous Piperazine Solutions with and without CO2 Loadings. Industrial & Engineering Chemistry Research 51, 12126-12134.

[5] Kim, I., Ma, X., Andreassen, J.-P., 2012. Study of the Solid-liquid Solubility in the Piperazine-H2O-CO2 System using FBRM and PVM. Energy Procedia Vol 23, 72-81.

[6] Mullin, J. W. Crystallization, 4 ed.; Elsevier Ltd, 2004

[7] Nývlt, J., Rychlý, R., Gottfried, J., Wurzelová, J. 1970. Metastable zone-width of some aqueous solutions. Journal of crystal growth, Vol 6, issue 2, January-Febrary, Pages 151-162

[8] S. Titiz-Sargut, J. Ulrich, 2002. Influence of Additives on the Width of the Metastable Zone Crystal Growth & Design, 2 (5), pp 371–374

[9] Barrett, P.; Glennon, B. 2002. Characterizing the metastable zone width and solubility curve using lasentec FBRM and PVM Chem. Eng. Res. Des. 2002, 80, 799–805

[10] O'Grady, D., Barrett, M., Casey, E., Glennon,B. 2007. The Effect of Mixing on the Metastable Zone Width and Nucleation Kinetics in the Anti-Solvent Crystallization of Benzoic Acid. Chemical Engineering Research and Design. Volume 85, Issue 7, Pages 945–952

[11] Vevelstad, S.J., Kim, I., Grimstvedt, A., Wiig, M., Aronu, U.E.. Study of degradation and heat of dissolution of solids in aqueous blend of AMP and KSAR loaded with CO_2. 13th International Conference of Greenhouse Gas Control Technologies, GHGT-13, 14-18 November 2016, Lausanne, Switzerland